Materials Science and Technology, 29 (2013) 1074-1079

Modelling the coarsening behaviour of TiC precipitates in high-strength, low-alloy steels

Jae Hoon Jang[a], Chang–Hoon Lee[b], Heung Nam Han[c], H. K. D. H. Bhadeshia[d,e], Dong–Woo Suh[d]

[a] *Technical Research Laboratories, POSCO, Pohang, Republic of Korea*

[b] *Korea Institute of Materials Science, Changwon, Republic of Korea*

[c] *Materials Science and Engineering, Seoul National University, Republic of Korea*

[d] *Graduate Institute of Ferrous Technology,Pohang University of Science and Technology, Pohang, Republic of Korea*

[e] *Materials Science and Metallurgy, University of Cambridge, U.K.*

Abstract

Some of the most modern automotive–sheet steels rely on a dispersion of fine precipitates based on TiC, generated during the major phase changes that occur as the rolled material is cooled to the coiling temperature. The coils themselves cool extremely slowly, thus leading to the coarsening of the precipitates and a loss of strength. Beginning with a calculation of the interfacial energy, the precipitate coarsening kinetics are modelled as a function of the stoichiometry of titanium and carbon. The purpose was to assess the influences of interface energy and Ti/C stoichiometry which limit the rate at which the dispersion coarsens by the diffusion of solute from the small to the larger particles. It is found that Ti/C ratio plays a critical role; a titanium concentration which is slightly less than required to combine with carbon leads to a dramatic reduction in the coarsening rate.

Keywords: HSLA steel, TiC, ferrite, coarsening, multicomponent diffusion

1. Introduction

Low–alloy steels precipitation hardened using the interphase precipitation mechanism [1] have seen a revival since the invention of the so–called *Nanohiten*, a strong sheet–steel which also is formable [2]. Interphase precipitates form at the transformation front as austenite decomposes into ferrite during hot–rolling, after which the sheet is coiled while still hot ($\approx 600°C$). These coils cool rather slowly to ambient temperature and this can cause the strengthening precipitates to coarsen.

Many of these new steels use (Ti,Mo)C as the main strengthening carbide, with the Mo added to retard coarsening [2–6]. The mixing of Mo and Ti on the metallic sublattice is not thermodynamically favoured, but its presence reduces the interfacial energy and hence the activation barrier to carbide nucleation [4]. During the subsequent coarsening stage, the role of Mo become passive due to the energetic disadvantage. Therefore, partial replacement of Ti by Mo effectively reduces the concentration of diffusion elements for the coarsening of carbide, leading to the observed retardation in these kinetic processes [4]. These ideas have been established experimentally and using first principles calculations backed by observations that the Mo concentration of the TiC decreases as the particle size increases. The influence of Mo addition on coarsening behaviour can be regarded as twofold; the role of the interfacial energy and the concentration of the diffusing element. This issue was once examined by Funakawa et al. [5] but in a qualitative way. The aim of the present work was, therefore, to investigate quantitatively which parameter is predominant in retarding carbide coarsening. Therefore, the coarsening characteristics of three hypothetical Fe–Ti–C steels as a function of the Ti/C ratios have been examined, taking into account the interfacial energy as a function of composition.

2. Interfacial Energy

Coarsening is driven by the interfacial energy between ferrite and TiC particles. There have been studies to determine the interfacial energy experimentally, but a wide range of values has been reported [7]. In the present work, the interfacial energy of TiC carbide in a Baker-Nutting orientation relationship with ferrite is evaluated using a method to estimate energies of

solid solutions based on the simple addition of neighbouring bonds [8] combined with the ability to count the number of broken bonds in each of the phases at the interface [9, 10]. The technique has been used to calculate the energy of coherent interphase boundaries in substitutional binary alloys [11–14]. Fig. 1 illustrates the atomic structure of coherent interfaces between Fe-TiC in the Baker-Nutting relationship, used to determine the coordination numbers of atomic bonds. When the concentration of solute atoms is assumed to be constant at the interfacial plane, the interfacial energy is calculated only from the difference in cohesive energies between the interfacial region and the bulk.

$$\sigma = E_{\alpha/\mathrm{TiC}} - \frac{1}{2}(E_{\alpha/\alpha} - E_{\mathrm{TiC/TiC}}) \tag{1}$$

where $E_{\alpha/\mathrm{TiC}}$ is the sum of bonding energies across the ferrite–TiC carbide interface, and $E_{\alpha/\alpha}$ and $E_{\mathrm{TiC/TiC}}$ are the sum of the bonding energies across the planes parallel to the interface in the ferrite and TiC carbide, respectively. On the assumption that the first and second nearest bonds contribute most to the interfacial energy, this can be rewritten as

$$\sigma = n_{\mathrm{Ti}}\{(Z^1_{\text{Fe-Ti}} + pZ^2_{\text{Fe-Ti}})\Delta e_{\text{Fe-Ti}} + (Z^1_{\text{M-C}} + qZ^2_{\text{M-C}})\Delta e_{\text{M-C}}\} \tag{2}$$

where n_{Ti} is the number of Ti atoms per unit area of interface, 'M' stands for a metal atom, $Z^n_{\text{A-B}}$ is the coordination number of n-th nearest bond between A and B atoms, and p and q are the ratios of the bonding energies of the first nearest neighbour to the second one in Fe-Ti and M-C, respectively. $\Delta e_{\text{Fe-Ti}}$ and $\Delta e_{\text{M-C}}$ are defined by

$$\Delta e_{\text{Fe-Ti}} = e^{\sigma}_{\text{Fe-Ti}} - \frac{1}{2}(e^{\alpha}_{\text{Fe-Fe}} + e^{\mathrm{TiC}}_{\text{Ti-Ti}}) \tag{3}$$

$$\Delta e_{\text{M-C}} = e^{\sigma}_{\text{Fe-C}} - e^{\mathrm{TiC}}_{\text{Ti-C}} \tag{4}$$

where $e^{\mathrm{i}}_{\text{A-B}}$ is the nearest bonding energy between A and B in phase i.

The interfacial coordination number of Ti and C atoms across the ferrite-carbide interface can be determined as $Z^1_{\text{Fe-Ti}} = 4$, $Z^2_{\text{Fe-Ti}} = 1$, $Z^1_{\text{M-C}} = 1$ and $Z^2_{\text{M-C}} = 4$ from Fig. 1. $\Delta e_{\text{Fe-Ti}}$ was evaluated from the regular solu-

tion constants for the face-centred cubic (FCC) structure assuming that $e^{\sigma}_{\text{A-B}} = e^{\alpha}_{\text{A-B}} = e^{\text{TiC}}_{\text{A-B}}$ [13, 15]. These assumptions are reasonable, because the strength of the nearest bond is dependent on the interatomic distance, and the contributions of nearest neighbours in FCC structure are much more than those which are second nearest neighbours.

The nearest bonding distance of Fe-Fe in BCC[1] and Ti-Ti in TiC structure, and Fe-Ti at interface is 2.49, 3.04 and 2.83 Årespectively [4]. The atomic distances Fe-Fe and Ti-Ti in the FCC structure are about 2.55 and 2.86, respectively, which are about 2.4% larger and 5.9% smaller than Fe-Fe in BCC and Ti-Ti in TiC based on the first principles calculations. Therefore, the strength of the Fe-Fe bond will be a little overestimated, while that of the Ti-Ti bond will be slightly underestimated. The Fe-Ti distance at the interface is between BCC and TiC structures; since the nearest bonding distance between Fe and Ti at the interface, 2.83 Å, is less than 6 % from those in the FCC structures of Fe and Ti, respectively, the bonding distance of nearest neighbour in solid-solution Fe-Ti with FCC structure will be comparable to that at the interface. The Fe-Ti bonding energy can be evaluated using the mixing enthalpy of regular solution model of the FCC structure as:

$$\Delta H_{mix} = N_A Z x(1-x)\Delta e_{\text{Fe-Ti}} \tag{5}$$

where N_A is the Avogadro's number, $Z = 12$ is the bulk coordination number of a metal atom in the FCC structure, x is the atomic fraction of solutes. Fig. 2 shows the enthalpies calculated for different temperature in Fe-Ti system of FCC structure. The enthalpy of mixing is evaluated at atomic fraction of 0.5:

$$\Delta H_{mix}(0.5) = H(0.5) - \frac{1}{2}\{H(0.0) + H(1.0)\} \tag{6}$$

where $H(x)$ represents the enthalpy of system corresponding to an atomic fraction x. It is noted that the reported regular solution constants are usually dependent on temperature but the degree of dependency is not significant [15]. The calculated $\Delta e_{\text{Fe-Ti}}$ is -0.707×10^{-20} J, which accords reasonably

[1]BCC and FCC stand for body–centred cubic and face–centred cubic respectively.

Materials Science and Technology, 29 (2013) 1074-1079

with -0.77×10^{-20} J obtained from Fe-Ti phase diagram [16], -0.53×10^{-20} J from the semi-empirical equation [15] or -0.89×10^{-20} J from the regular solution constants of BCC phases [13].

Fig. 3 illustrates schematically the procedure for the evaluation of the bonding energy between Fe-C and Ti-C interactions, based on the enthalpy difference of two systems with the same number of Fe and Ti atoms using ThermoCalc with TCFE6.2 databases. The first is the combination with the B1 structure FeC and FCC Ti, where all carbon atoms that bond with Fe are calculated. The second one consists of B1 structure TiC and nonmagnetic FCC Fe, where carbon atoms bond with Ti atoms. The atomic bonding energy is evaluated as,

$$\Delta H_{\text{M-C}} = NZ\Delta e_{\text{M-C}} \tag{7}$$

where N is the number of Fe atoms in the system, $Z = 6$ is the coordination number of C atom with nearest metal atom. The calculated $\Delta e_{\text{M-C}}$ is 7.15×10^{-20} J.

The ratio of the first nearest bonding energy to the second one in metal atoms, p, is reported to be between 3/4 and 1 for BCC crystals [17]. It is relatively small for FCC structure because the bonding energy is highly dependent on the separation between two atoms. Since the second nearest distance of metal atoms from carbon is $\sqrt{5}$ times larger than the first one in the interface structure, the q can be assumed to be negligibly small. The calculated interfacial energy changes from 409 mJ m^{-2} for $p = 1.0$ to 489 mJ m^{-2} for $p = 0.5$. This interfacial energy includes not only the contribution from the chemical bonding energy but also from the structural strain energy, since the thermodynamic databases were assessed from the experiments.
The chemical term to interfacial energy were reported to be 339 mJ m^{-2} and 256 mJ m^{-2} for TiC and MoC with first-principles calculation [4]. The strain energy contributions in the interfacial energy are evaluated to be 154 mJ m^{-2} and 83 mJ m^{-2} on the assumption that the strain energy is localized to one atomic layer of ferrite and MC type structure using following equation, respectively.

$$\sigma_s = \frac{2\times E_s}{a_\alpha^2\times N_A} \tag{8}$$

where σ_s is the strain energy contribution for the interfacial energy, E_s is the strain energy from the reported values [4], a_α is the lattice parameter of ferrite and N_A is the Avogadro's constant. The interfacial energies for TiC and MoC are 493 mJ m^{-2} and 339 mJ m^{-2} taking into account both structural and chemical contributions. It shows a reasonable agreement with the present calculation.

3. Coarsening Theory

A widely accepted theory for coarsening of a small fraction of precipitates, controlled by diffusion is given by the Lifshitz, Slyozov and Wagner (LSW) [18–20]:

$$\overline{r}(t)^n - \overline{r}(0)^n = \frac{8}{9}\frac{\sigma V_m^2 D C_e}{RT}t \tag{9}$$

where t is time, $\overline{r}$ is the average radius of the particles, σ is interfacial energy per unit area between particles and matrix, D is a diffusion coefficient of element controlling the coarsening, C_e is the equilibrium concentration of the solute in the matrix through which it diffuses and V_m is the molar volume of the particle [20]. n is a constant determined by coarsening mechanism; $n = 2$ for interface migration coarsening, $n = 3$ for bulk diffusion, $n = 4$ for grain boundary diffusion and $n = 5$ for dislocation diffusion [19–21]. The particle size distribution function was also derived by the Lifshitz and Slyozov [19], which predicts that the scaled distribution should eventually reach a universal form which is independent of all material parameters. The radius of the biggest particle is then 1.5 times larger than the average one.

Spherical TiC particles with an average radius of 2 nm and a size distribution given by the LSW theory were assumed for coarsening simulation [18–20]. The alloy systems considered are Fe-0.04C-0.2Ti, Fe-0.04C-0.18Ti and Fe-0.04C-0.15Ti (in wt%), which are design to reflect the decrease in Ti concentration when alloying element having passive role during coarsening replaces Ti and thus to examine the influence of stoichiometric balance between C and Ti on the coarsening rate. As an interfacial energy, 425 mJ m^{-2} evaluated with $p = 0.8$ and $q = 0.0$, is employed. Additionally, calculation is also conducted with 256 mJ m^{-2}, which can be regarded as lower bound

value relieved with Mo addition [4]. The calculation was done for ageing at 700 °C for 1.0×10^5 s.

The equilibrium concentrations and diffusivity of Ti in ferrite were obtained from the TCFE6.2 and MOBFE1 databases [22, 23]. Fig. 4 shows the ternary phase diagram of the Fe-Ti-C system at 700 °C. The concentration of Ti in ferrite that is in equilibrium with TiC follows a straight line with a slope of approximately -1. This indicates a constant solubility product of Ti and C at a given temperature. The open rectangle and circle in BCC + TiC region identify the 0.04C-0.2Ti and 0.04C-0.15Ti compositions, respectively. The open symbols on the BCC/BCC + TiC phase boundary represent the composition of ferrite in equilibrium with TiC. Much of the C in 0.04C-0.2Ti alloy bound with Ti as TiC but there is excess carbon in the case of the 0.04C-0.15Ti alloy, leaving very little Ti in solution within the ferrite. As a result, the equilibrium mass fractions of Ti in ferrite at 2.1×10^{-4} and 1.5×10^{-8} in 0.04C-0.2Ti and 0.04C-0.15Ti alloy, respectively, differ dramatically between the two alloys.

The diffusivity of solute in ferrite also controls the coarsening rate. Fig. 5 shows the calculated diffusivities of Ti and C as a function of temperature, based on the TCFE6.2 and MOB2 databases for 0.2Ti-0.04C alloy. The diffusivity of C is $10^6 \sim 10^7$ times higher than Ti at the temperature of interest, so it is assumed that Ti diffusion exercises rate–control. The calculated parameters for 700°C are listed in Table 1.

The assumption that Ti diffusion in ferrite controls coarsening kinetics in the treatment of LSW using Eq. 9 leads to the simple interpretation that the compositions at the interface are given by a tie–line of the equilibrium phase diagram. This may not be justified in a system undergoing phase transformation where the fluxes of the fast and slow diffusing species must keep pace in order to maintain local equilibrium at the interface. [24–26].

To assess this issue, DICTRA simulations for coarsening with multicomponent diffusion and capillarity were carried out [27]. The procedure involves tracing the coarsening rate of the largest particle in the system assuming that the size distribution follows the LSW theory. Since the maximum particle size is 1.5 times larger than the average, the initial radius r_p is set to be 3 nm for the simulation, which is 1.5 times the average size. The radius of spherical cell r_v of the ferrite which surrounds the particle is determined from mass

balance as:

$$\frac{(4/3)\pi r_p^3}{(4/3)\pi r_v^3} = \text{volume fraction of precipitate.} \quad (10)$$

Table 2 summarises the calculated equilibrium concentration at 700°C as initial conditions for DICTRA simulation. $c_{\mathrm{Ti}}^{\alpha\rho}$ and $c_{\mathrm{C}}^{\alpha\rho}$ are the concentrations of Ti and C in ferrite, which are equilibrium with TiC, and $c_{\mathrm{Ti}}^{\rho\alpha}$ and $c_{\mathrm{C}}^{\rho\alpha}$ are the corresponding concentrations of Ti and C in the precipitate, which are equilibrium with ferrite. The calculated phase fractions of ferrite and TiC, and the initial cell sizes (Eq. 10) are listed in Table 3.

4. Influencing parameter on TiC coarsening

Table 1 indicates that the parameters used in the LSW theory, i.e., the diffusivity and the equilibrium concentration of Ti in ferrite, molar volume of TiC phase, increase as the concentration of Ti increased. It is noted that the change in Ti concentration in ferrite, C_e, is most significant among them and has a critical influence on the coarsening rate within the range of Ti content investigated.

Fig. 6(a) shows the evolution of precipitate mean radius calculated using the LSW model. The particle radius at 10^5 s of 0.04C-0.2Ti alloy with interfacial energy $\sigma = 425$ mJ m^{-2} is 2.54 nm. They are 2.13 and 2.00 nm for 0.04C-0.18Ti and 0.04C-0.15Ti alloys, respectively. The coarsening rate in 0.04C-0.15Ti steel is negligible because $c_{\mathrm{Ti}}^{\alpha\rho}$ is 1/100 times less than in the other alloys. This is because for 0.04C-0.15Ti, the concentration of C is greater than required to consume almost all of the Ti to form the carbide. Consequently, the coarsening rate is very sensitive to the variation in the atomic ratio of Ti to C, which determines $c_{\mathrm{Ti}}^{\alpha\rho}$. Fig. 6(a) also indicates the influence of interfacial energy on the coarsening rate. As expected from Eq.9, the coarsening is retarded as the interface energy decreases. Comparing the effect of interface energy and diffusive element concentration in matrix, the latter is more potent regarding to on the retardation of coarsening. For example, the decrease of Ti concentration in ferrite accompanying 20 % of replacement of Ti by Mo suppresses the coarsening more significantly than the reduction of interfacial energy by complete substitution of Ti. It suggests

that stoichiometry of Ti and C should be precisely controlled to maintain the strengthening effect by fine TiC precipitation. Even though lack of experimental results on the alloy system in this study, Funakawa et al. [5] have reported that just decrease of Ti concentration without addition of Mo could make the coarsening behavior similar to that of Mo-added one, which is coherent to the present work. Fig. 6(b) shows the corresponding coarsening calculations using DICTRA. The particle radii at 10^5 s of 0.04C-0.20Ti with σ =425 mJ m^{-2} is 2.51 nm. They are calculated to be 2.15 and 2.00 nm for 0.04C-0.18Ti and 0.04C-0.15Ti alloys, respectively. These accord reasonably with the estimates using the LSW theory and assuming that only the diffusion of Ti needs to be considered. Figs 7 and 8 show how the concentrations of Ti and C vary across the interface for 0.04C-0.2Ti and 0.04C-0.18Ti alloys with σ =425 mJ m^{-2}, as a function of time at temperature. The interface composition at 0 s corresponds to the equilibrium values given in Table 2. During coarsening, the concentrations $c_{\mathrm{i}}^{\alpha\rho}$ are influenced by capillarity, i.e., the equilibrium between ferrite and the carbide changes with particle size since a smaller particle has a greater free energy by virtue of the amount of surface per unit volume. This is why the composition $c_{\mathrm{i}}^{\alpha\rho}$ changes as the time (and particle size) increase but its effect on coarsening rate is not significant as we know from Figs. 6(a) and (b).

5. Summary

With respect to the partial replacement of titanium by molybdenum, it was reported to have twofold effects on the retardation of coarsening by changing the interface energy between TiC particle and ferrite matrix and the diffusive solute concentration in matrix for coarsening. Both the LSW results and DICTRA simulations indicate that having a slight excess of carbon can dramatically reduce the coarsening rate of TiC particles in a ferrite matrix for the Fe–Ti–C system. This is because the concentration of titanium in the ferrite at the interface becomes so small that the diffusion gradients which drive coarsening become extremely shallow. It demonstrates that Ti/C stoichiometry plays more influencing role. One reason why it has a profound influence on coarsening is the strong affinity that titanium has for c, leading to the formation of TiC without involvement of iron–titanium carbides. Thus, the conclusions reached here may not apply for relatively weak carbide forming solutes such as chromium, where mixed iron–chromium carbides are

common.

We acknowledge Professor Chong Soo Lee for the provision of laboratory facilities at GIFT. This work was supported by the Steel Innovation Programme by POSCO and the World Class University programme (Project No. R32-2008-000-10147-0) by the National Research Foundation of Korea.

References

[1] R. W. K. Honeycombe, Metal Science 14 (1980) 201–214.

[2] K. Seto, Y. Funakawa, S. Kaneko, JFE GIHO (2007) 28–33.

[3] H. W. Yen, C. Y. Huang, J. R. Yang, Scripta Materialia 61 (2009) 616–619.

[4] J. H. Jang, C. H. Lee, Y. U. Heo, D. W. Suh, Acta Materialia 60 (2012) 208–217.

[5] Y. Funakawa, K. Seto, Tetsu–to–Hagane 93 (2007) 49–56.

[6] C. Y. Lee, D. H. Choi, Y. M. Yeon, K. Song, S. B. Jung, Science and Technology of Welding and Joining 14 (2009) 216–220.

[7] S. Shahandeh, S. Nategh, Materials Science and Engineering A 443 (2007) 178–184.

[8] R. Becker, Annalen der Physik 424 (1938) 128–140.

[9] J. K. Mackenzie, A. J. W. Moore, J. F. Nicholas, Journal of Physics and Chemistry of Solids 23 (1962) 185–196.

[10] J. K. Mackenzie, J. F. Nicholas, Journal of the Physics and Chemistry of Solids 23 (1962) 197–205.

[11] R. Ramanujan, J. Lee, H. Aaronson, Acta Metallurgica et Materialia 40 (1992) 3421–3431.

[12] S. Dregia, Wynblatt, Acta Metallurgica et Materialia 39 (1991) 771–778.

[13] Z. Yang, M. Enomoto, Materials Science and Engineering A 332 (2002) 184–192.

[14] Z. Yang, M. Enomoto, Metallurgical & Materials Transactions A 32 (2001) 267–274.

[15] Y.-S. Yang, K.-J. Son, S.-K. Cho, S.-G. Hong, S.-K. Kim, K.-H. Mo, Science and Technology of Welding and Joining 6 (2001) 397–401.

[16] K. C. H. Kumar, P. Wollaiits, L. Delaey, Calphad 18 (1994) 223–234.

[17] J. Nicholas, Austrailian Journal of Physics 21 (1968) 21–34.

[18] G. Greenwood, Acta Metallurgica 4 (1956) 243–248.

[19] I. M. Lifshitz, V. V. Slyozov, Journal of the Physics and Chemistry of Solids 19 (1961) 35–50.

[20] C. Wagner, Zeitschrift für Elektrochemie 65 (1961) 581–591.

[21] A. Ardell, Acta Metallurgica 20 (1972) 61–71.

[22] B. Sundman, B. Jansson, J. O. Andersson, CALPHAD 9 (1985) 153–190.

[23] J. O. Andersson, T. Helande, L. Hoglund, P. Shi, B. Sundman, CALPHAD 26 (2002) 273–312.

[24] D. E. Coates, Metallurgical Transactions 3 (1972) 1203–1212.

[25] D. E. Coates, Metallurgical Transactions 4 (1973) 1077–1086.

[26] N. Fujita, H. K. D. H. Bhadeshia, M. Kikuchi, Modelling and Simulation in Materials Science and Engineering 12 (2004) 273–284.

[27] J. O. Andersson, J. A. gren, Journal of Applied Physics 72 (1992) 1350–1355.

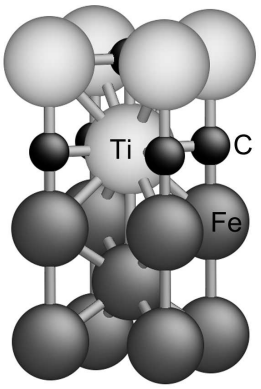

Figure 1: Atoms showing the Fe-TiC interface structure with a Baker-Nutting orientation relationship.

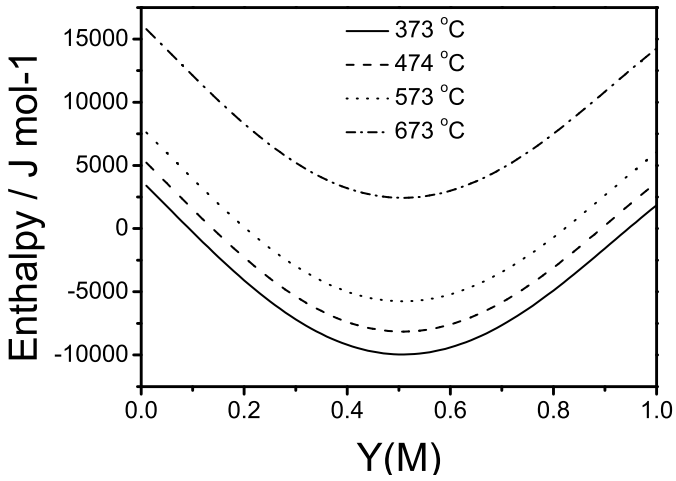

Figure 2: The calculated enthalpy of mixing of FCC at different temperatures versus atomic fraction of titanium. The value corresponding to 0.0 represents FCC Fe and 1.0 represents FCC Ti.

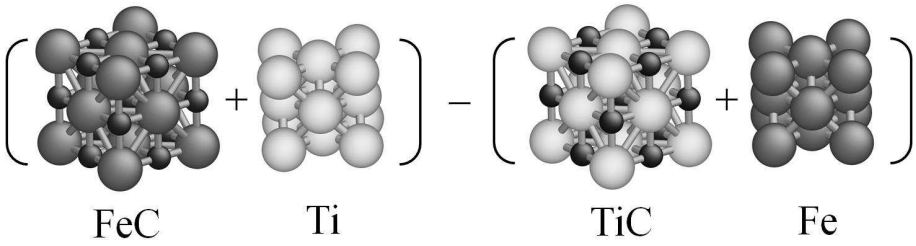

Figure 3: Schematic illustration for the evaluation of bond energy between Fe-C interaction and Ti-C interaction. The system energies are evaluated using ThermoCalc with TCFE6.2 database.

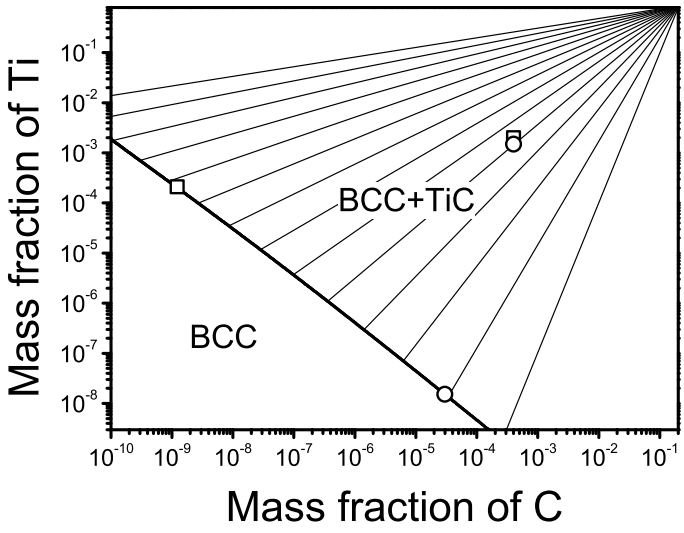

Figure 4: Calculated ternary phase diagram of Fe-Ti-C system at 700°C. The concentrations are in mass fractions. The blank rectangle and circle in two phase region correspond to 0.04C-0.2Ti wt% and 0.04C-0.15Ti wt%, respectively. The blank rectangle and circle on the lines between BCC(ferrite) phase region and two phase region indicate equilibrium concentrations in ferrite.

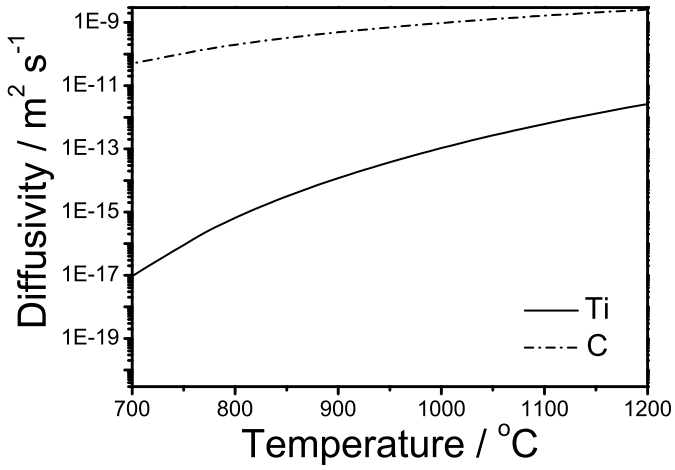

Figure 5: Calculated diffusivities in BCC phase of Ti and C in 0.04C-0.2Ti system from MOBFE1 database as a function of temperature.

Table 1: Calculated diffusivity, Ti equilibrium concentration in matrix and molar volume of precipitates for one mole of Ti in precipitates at 700°C . The values of C_e are converted to number of moles per volume using mole fraction of Ti in matrix and molar volume of matrix.

wt%	D / m s^{-2}	C_e / mol m^{-3}	V_m / m^3 mol^{-1}
0.04C-0.20Ti	9.3041×10^{-18}	33.80	1.2452×10^{-5}
0.04C-0.18Ti	9.2739×10^{-18}	7.9383	1.2442×10^{-5}
0.04C-0.15Ti	9.2648×10^{-18}	0.0241	1.2407×10^{-5}

Table 2: Calculated equilibrium mass fractions at 700°C. $c_{\mathrm{Ti}}^{\alpha\rho}$ and $c_{\mathrm{C}}^{\alpha\rho}$ are the matrix compositions of Ti and C, which are equilibrium with precipitate phase. $c_{\mathrm{Ti}}^{\rho\alpha}$ and $c_{\mathrm{C}}^{\rho\alpha}$ are the precipitate compositions of Ti and C, which are equilibrium with ferrite.

wt%	$c_{\mathrm{Ti}}^{\alpha\rho}$	$c_{\mathrm{C}}^{\alpha\rho}$	$c_{\mathrm{Ti}}^{\rho\alpha}$	$c_{\mathrm{C}}^{\rho\alpha}$
0.04C-0.20Ti	2.117×10^{-4}	1.464×10^{-8}	0.8173	0.1827
0.04C-0.18Ti	4.971×10^{-5}	7.272×10^{-8}	0.8140	0.1860
0.04C-0.15Ti	1.515×10^{-7}	3.375×10^{-5}	0.8037	0.1963

Table 3: Calculated equilibrium volume fractions of ferrite and carbide in volume fraction at 700°C. r_v is the radius of the total system which matches the volume fraction of precipitate with 3 nm radius.

wt%	ferrite	precipitate	r_v / nm
0.04C-0.20Ti	0.9965	3.55×10^{-3}	19.66
0.04C-0.18Ti	0.9965	3.47×10^{-3}	19.81
0.04C-0.15Ti	0.9970	2.97×10^{-3}	20.87

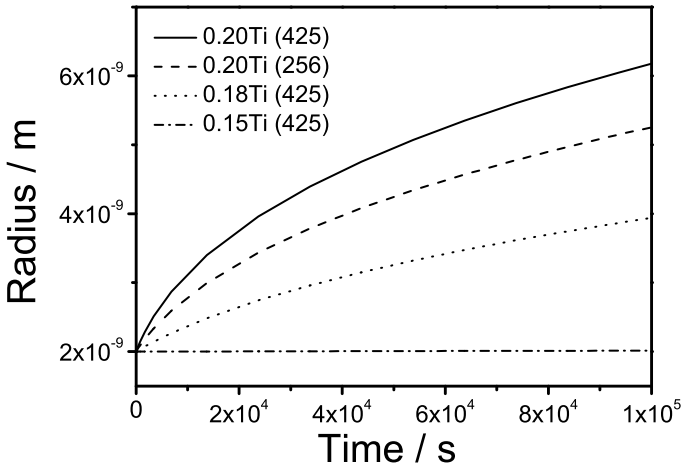

(a)

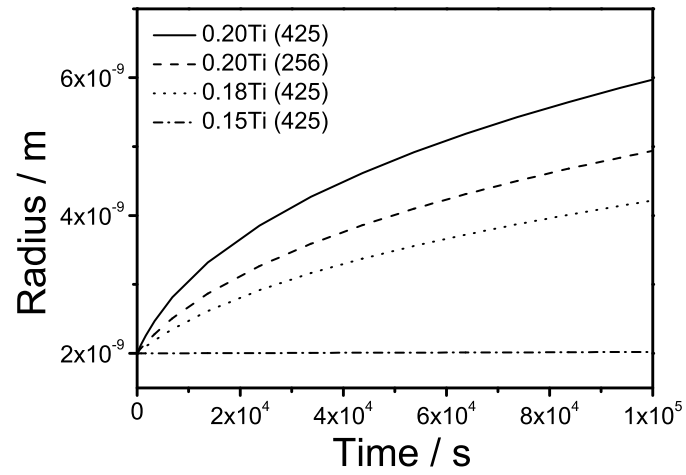

(b)

Figure 6: Variation of precipitate mean radius calculated using (a) LSW model and (b) DICTRA software toexhibit time dependent coarsening of the TiC phase in 0.04C-0.2Ti, 0.04C-0.18Ti and 0.04C-0.15Ti wt% system at 700°C.

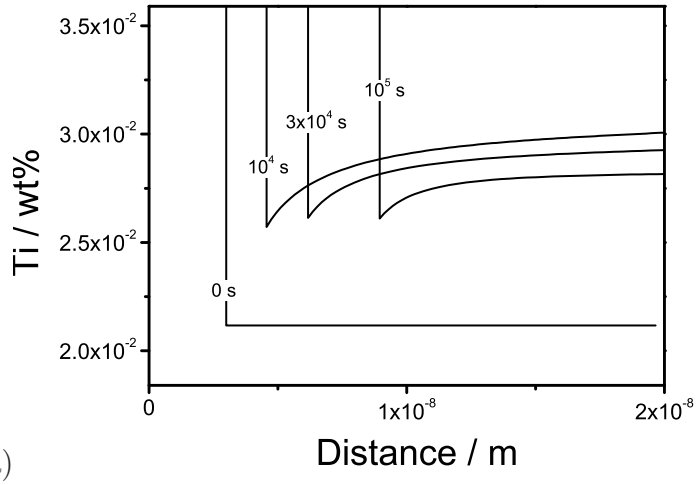

(a)

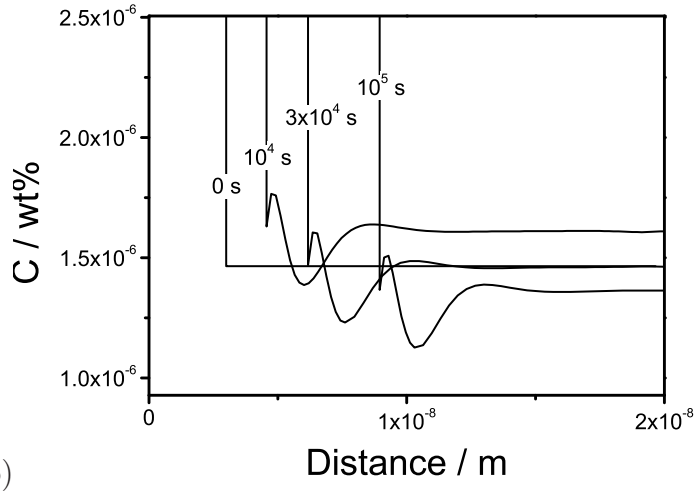

(b)

Figure 7: Concentration-distance profile for 0.04C-0.20Ti wt% with σ =0.425 J m^{-2}, showing distribution of (a) Ti and (b) C across the interface between precipitate and ferrite matrix at different time intervals.

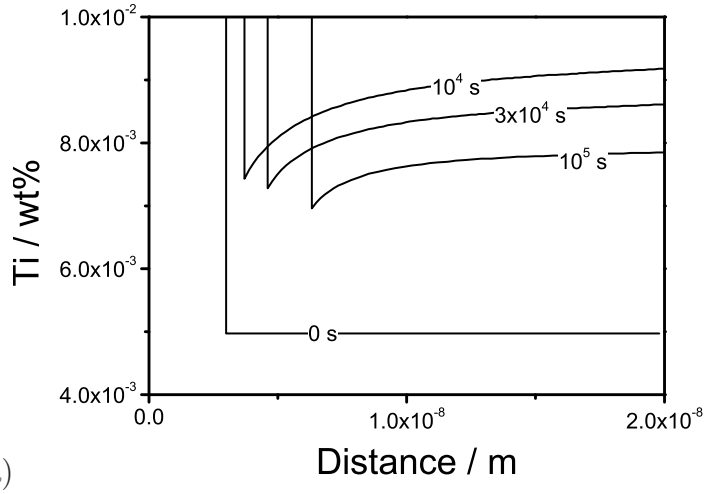

(a)

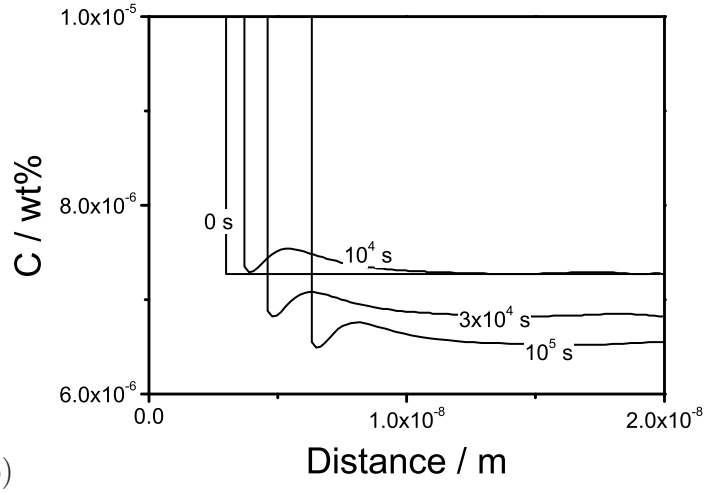

(b)

Figure 8: Concentration-distance profile for 0.04C-0.18Ti wt% with σ =0.425 J m^{-2}, showing distribution of (a) Ti and (b) C across the interface between precipitate and ferrite matrix at different time intervals.